Differentiating COVID-19 Cases from Others by an Anatomy Similarity-Inspired Sensitive Merit from CT Images

Yongfeng Gao, Marc Pomeroy, Weiguo Cao, Siming Lu, Fangfang Han, Luhao Wang, Mu Chen, Junqi Sun, Hong Xie, and Zhengrong Liang

2020 IEEE Nuclear Science Symposium and Medical Imaging Conference (NSS/MIC) | 978-1-7281-7693-2/20/$31.00 ©2020 IEEE | DOI: 10.1109/NSS/MIC42677.2020.9508088

***Abstract* — Computed tomography (CT) of COVID-19 manifests a relatively global effect through the whole lungs, like peripheral ground glass, consolidation, reticular pattern, nodules etc. This characteristic effect renders the difficulties in differentiating COVID-19 from the normal body or other lung diseases by CT. This work presents a novel method to relieve the difficulties by reducing the global effect through the 3D whole lung volume into 2D-like domain. The hypothesis is that the lung tissue shares the similar anatomic structure within a small lung sub-volume for normal subjects. Therefore, the anatomic land-markers along the z-axis, denoted as Lung Marks are used to eliminate axial variable. Our experiments indicated that 30 Lung Marks are sufficient to eliminate the axial variable. The method computes texture measures from each 2D-like volumetric data and maps the measures on to the corresponding Lung Mark, resulting in a profile along the z-axis. The difference of the profiles between two different abnormalities is the proposed sensitive merit to differentiate COVID-19 cases from others in CT images. 48 COVID-19 cases and 48 normal screening cases were used to test the effectiveness of the proposed sensitive merit. Intensity and gradient based texture descriptors were computed from each axial cross image at the corresponding Lung Mark along the z-axis. Euclidean, Jaccard and Dice distances are calculated to generate the profiles of the proposed sensitive merit. Consistent results are observed across texture descriptor types and distance types in the texture measure between the normal and COVID-19 subjects. Uneven Profiles demonstrate the variation along the z-axis. With Lung Mark, the variation of texture descriptor has been reduced prominently. The Gradient based descriptor is more sensitive. Individual Haralick features analysis shows the 2nd and 10th dimensions are most distinguishable.**

Manuscript received November 13, 2020. This work was partially supported by the NIH/NCI grant #CA143111 and #CA206171. * indicates corresponding authors.

Y. Gao, M. Pomeroy and W. Cao, Siming Lu are with the Department of Radiology, Stony Brook University, Stony Brook, NY 11794, USA.

F. Han is with the School of Biomedical Engineering, Southern Medical University, Guangzhou, Guangdong, 510515, China.

L. Wang is with the School of Electrical Engineering and Computer Science, Pennsylvania State University, University Park, PA 16802 USA.

M. Chen is with Innovision Imaging Laboratory INC, Durham, NC, 27709, USA and Duke Kunshan University, Kunshan, Jiangsu, 215316, China.

J. Sun is with the Department of Radiology, Yuebei People's Hospital, Shaoguan, Guangdong, 710049, China.

*Z. Liang is with the Departments of Radiology, Biomedical Engineering, Computer Science, and Electrical Engineering, Stony Brook University, Stony Brook, NY 11794, USA (e-mail: Jerome.Liang@sunysb.edu).

*H. Xie is with the Department of Radiology, The Affiliated Hospital of Guizhou Medical University, Guiyang, 550004, China. (e-mail: doctorxie2007@yeah.net).

I. Introduction

CORONAVIRUS disease 2019 (COVID-19) outbreak has spread around the world since the beginning of 2020, causing global public health emergency. Real time polymerase chain reaction (RT-PCR) testing is the golden standard for COVID-19 diagnosis. However, its sensitivity can be as low as 70% [1-2]. With higher sensitivity, the computed tomography (CT) has been reported an effective supplement to RT-PCR test and suggested to be as a necessary tool for diagnosis [3]. Although CT can provide almost the real-time report, reviewing images is still a huge workload for the radiologist. Therefore, it is of big impact using artificial intelligence to assistant radiologist making a decision, especially in the shortage of medical care.

CT images of COVID-19 show a relatively global effect through the whole lungs. As reported in many works [4-6], the common manifestations in CT images are ground glass opacities, consolidation, crazy paving, reversed halo, rounded nodules, etc. The abnormality could localize at only partial lung region or distribute along the whole lung region. This characteristic effect renders the difficulties in differentiating COVID-19 such as huge volumetric data for artificial neural network based model or large feature variation for tree-based model. For example, assuming the lung height is 30cm and the CT image thickness is 1mm, there will be 300 slices for the whole lung region. It will be challenging to deal with the three-dimensional (3D) data directly in the neural network [7] either in the network design or training.

This work presents a novel method to relieve the difficulties mentioned above. An anatomic similarity inspired land-marker Lung Marks are proposed to reduce the global effect through the 3D whole lung volume into two-dimension (2D) domain under the hypothesis that lung tissue shares the similar anatomic structure within a small lung sub-volume for normal subjects. By this method, the feature variation can be reduced significantly.

The reminder of this paper is organized as follows. Section II describes the proposed Lung Marks and sensitive metrics for classification. Section III presents experimental design and results. Discussion and Conclusions are drawn in Section IV.

II. Methods

A. Lung Marks

As introduced above, the proposed method aims to reduce

the global effect by converting the 3D whole lung volume into 2D domain. Intuitively, the lung parenchyma within small volume won't change too much. In the previous studies [8, 9], it is observed that the lung tissue texture for the neighboring seven slices does not change too much. Beyond that local region, the tissue texture may vary. Figure 1 presents the lung textures of the neighboring six slices, where the lung texture is the Markova Random Filed weights extracted from tissue region [10]. Inspired by this observation, we propose the anatomic land-markers along the z-axis, denoted as Lung Marks to label each slice. Therefore, the cross section at each Lung Mark i.e., z location has similar texture patterns for normal subjects. By doing so, we can eliminate axial variable and convert the 3D data into 2D-like domain.

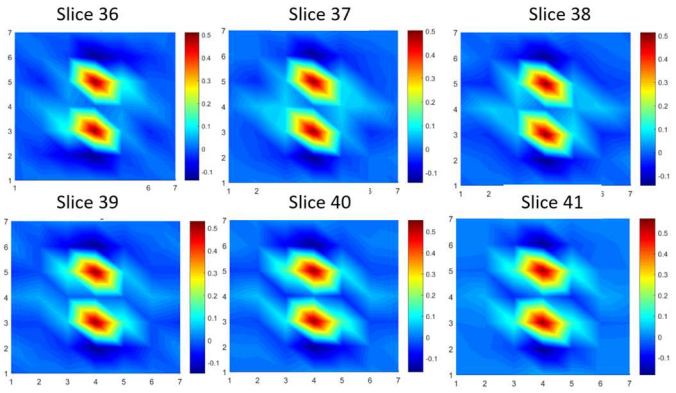

Fig. 1. Lung textures of neighboring six slices.

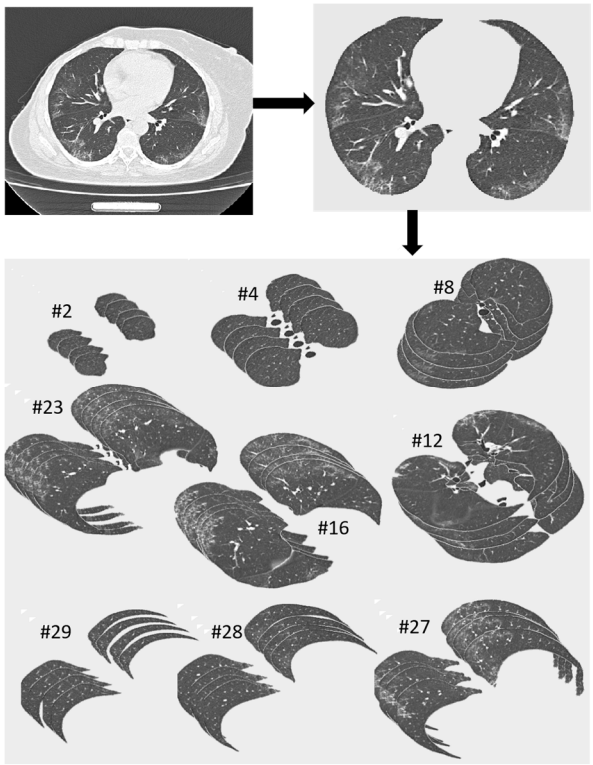

Fig. 2. Flowchart of the proposed method. The number in the figure is the Lung Mark of those slices.

Figure 2 presents the flowchart of the proposed merit Lung Mark. The number in this figure is the Lung Mark of those slices. Firstly, the CT images will be segmented to obtain the lung volume. Then the neighboring slices will be grouped according to their Lung Mark label. The slices of the same Lung Mark share the similar anatomy structure as shown in Fig. 1. Our experiments indicate that 30 Lung Marks are sufficient to eliminate the axial variable. Each Lung Mark may contain less than 1 cm high Lung using the same assumption that the whole lung is of 30 cm height.

The segmentation stage includes two steps: (1) automatic segmentation using the previous reported vector quantization VQ algorithm. Each voxel inside the image would be assigned to one specific tissue based on the classification once the number of tissues was set, e.g., R=4 to represent lung, bone, fat and muscle for the chest CT. In the classification, the center of each class (i.e. the mean value of the intensity within one specific tissue) would be updated once a new voxel was added and become the new reference point for the to-be-classified voxel. (2) automatic morphological operations. This operation enlarges the segmented lung parenchyma to include any the juxta-pleural abnormalities.

B. Texture Descriptors from Lung Mark labeled Data

The method computes texture measures from each 2D-like cross sections and maps the measures on to the corresponding Lung Mark, resulting in a profile along the z-axis. The difference of the profiles between two different abnormalities is the proposed sensitive merit to differentiate COVID-19 cases from others in CT images.

To describe the texture descriptors from Lung Mark labeled data, it is necessary to extract some texture features as their representation. In this topic, there have existed many methods such as local binary pattern (LBP) [11], Weber local descriptor (WLD) [12], Gabor [13], wavelet [14], GLCM [15,16], gray level run-length matrix (GLRLM) [17], gray level size zone matrix (GLSZM) [18], neighboring gray-level dependence matrix (NGLDM) [19] and so on. In this article, we choose GLCM to produce texture pattern. The definition of GLCM could be found in [15]. This choice is a deliberate decision after full investigations according to GLCM method and its properties as follows:

- 2D squared patterns: GLCM is a 2D histogram which represents some pixel-pair distributions along with different directions. Compared with histogram-based descriptors such as LBP, WLD, NGLDM and wavelet entropy, these pixel pair patterns extract more structural information which is an important texture representation. Moreover, this pattern is expressed by a squared array which might provide a lot of conveniences as the input of some deep learning packages [7].
- Less effects by the boundaries and postures: As an important geometrical feature, boundaries represent some global structures of objects. However, some objects, such as polyps and lung nodules, have more tendency to be expressed by their textures than boundaries and postures. Pixel pairs contains significant clues of local patterns or image details which are independent of the two geometric factors. Moreover, GLCM's local structure also contains more direction information than GLRLM, GLSZM and NGLDM.

- Scale and rotational robustness: Since GLCM employ pixel pair distribution to represent texture patterns, the scale factor could be removed by its normalization. So, it shares scale robustness with other typical methods listed above. Beyond that, GLCM contains complete direction information around one concerned pixel. Therefore, it has much stronger description under rotational transformation than WLD, wavelet, Gabor and so on.

In 2D images, the GLCM is defined as the follows:

$$M_{i,j}(d,\theta,s) = \sum_{\substack{m=1,\\ m\leftarrow m+s}}^{M} \sum_{\substack{n=1\\ n\leftarrow n+s}}^{N} \begin{cases} 1 & I(m,n) = i, I\big((m,n) + d * \theta\big) = j \\ 0 & otherwise \end{cases} \tag{1}$$

where I represents the grayscale image, (M,N) is the image size, i and j are a pair of image pixels, d is the displacement between two pixels along the direction θ, and s represents the stride. A pictorial illustration of Eq. (1) is shown in Fig. 3(a). When s=d=1, GLCM is defined as the GLCM model. Therefore, GLCM seeks to expand the traditional GLCM using multi-scale analysis. This model provides a new tool to capture more texture patterns. A typical example of GLCM calculation is shown by Fig. 3(b) where stride is equal to 1. For 3D volumetric image data, the GLCM model is similar to the 2D model except that two directions are used in its coefficients. In our case, the data at each Lung Mark is still 3D. In total, GLCM will be extracted from thirteen directions.

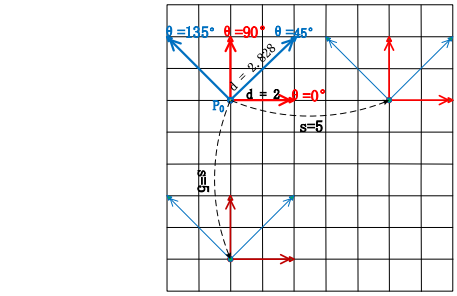

(a)

	0	1	2	3	4	5	6	7
0	0	0	0	0	0	0	0	0
1	0	0	2	0	0	0	0	0
2	0	1	1	2	0	0	2	1
3	0	0	1	1	0	0	2	1
4	0	0	0	0	0	0	0	0
5	0	0	0	0	0	0	0	0
6	0	0	0	0	0	0	0	1
7	0	1	3	0	0	0	1	0

(b)

Fig. 3. GLCM calculation. (a) Calculation of GLCM where d represents displacement, θ is the direction, s is stride (or scale), p_0 is the concerned point; (b) A GLCM illustration of 2D arrays where the gray level is set to be 8, direction (θ)= 0°, displacement(d)=1, and s=1.

Two groups of GLCMs are calculated from two image domains, i.e. intensity and gradient. Every group include 13 matrices which are generated from the 1st ring neighbor around one concerned voxel with 13 independent directions and 32 gray levels. In gradient based texture descriptor calculation, we employ Sobel operator to calculate full gradient information, i.e. magnitude, azimuth and polar angle, which form a 3D vector to calculate co-occurrence matrices where their gray levels are set to be (4,2,4) to generate new digital voxels [20]. Since the gradient magnitude varies in the range of [-10000, 10000], we employ n-th root mapping to normalization the magnitude where n in {1, 2, 3}.

Every group produces four type of descriptors including Haralick measures, traditional features, extended Haralick measures and extended Haralick features [15,16]. Haralick measures extract 14 measures from GLCM to represent the whole image or volume while 30 measures are used in extended Haralick measures. As our previous study, two measures, i.e. 21 and 30, is excluded since the 21st is equal to 0 and the 30th is equal to the 25th [20].

C. Texture Descriptors Distance

As the guideline of our idea, the normal texture descriptors of Lung Marks are treated as the baseline which is implemented to measure the difference from the COVID19 images. There are many types of distances as dissimilarity measures. We choose three of them as our measurement, i.e. Euclidean distance, Jaccard distance [21] and Dice distance [22]. Suppose two descriptors $F_1 = (v_{11}, \cdots, v_{1N})$ and $F_2 = (v_{21}, \cdots, v_{2N})$. The definitions of three measures are given as follows:

Euclidean distance:

$$D_E = \sum_{i=1}^{N} (v_{2i} - v_{1i}) \tag{2}$$

Jaccard distance:

$$D_J = 1 - \frac{|F_1 \cap VF_2|}{|F_1 \cup F_2|} \tag{3}$$

Dice distance:

$$D_D = 1 - \frac{2*|F_1 \cap F_2|}{|F_1| + |F_2|} \tag{4}$$

where ∩ represents set intersection, ∪ is the union of the two sets, and $|\cdot|$ denotes the variable numbers in one set.

Suppose that $F = \{F_1, F_2, \cdots, F_M\}$ is the descriptor set, $F_i \in F$ is its i-th descriptor and $F_i = (v_{i1}, \cdots, v_{iN})$, then F is a M*N matrix. Its j-th column could be donated by $V_j = (v_{1j}, \cdots, v_{Mj})$. The descriptor normalization is performed firstly before dissimilarity calculation as the following,

$$v_{ij}^n = \frac{2*v_{ij} - (\max(V_j) + \min(V_j))}{\max(V_j) - \min(V_j)} \tag{5}$$

where v_{ij} is the i-th variable of V_j, $\max(V_j)$ represent the maximum of V_j, and $\min(V_j)$ donates the minimum of V_j.

Since $\min(V_j) \le v_{ij} \le \max(V_j)$, it is easy to get

$$-1 \le v_{ij}^n \le 1 \tag{6}$$

Therefore, all variables in matrix F are mapped into [-1,1]. Euclidean distance is the mostly used measurement in our life and easy to compute. To calculate the D_J and D_D, v_{ij}^n is digitalized by the uniform scaling method with 10 bins. The digitalized descriptors are put into Eq (3) and Eq (4) to calculate the Jaccard distance and Dice distance between the COVID19 descriptors and the baseline.

III. Experiments and Results

Following the flowchart in method section, we evaluate the

proposed method based on two datasets: 48 COVID-19 cases and 48 normal screening cases. Then all slice images will be segmented and labeled by the Lung Mark. Texture descriptors will be calculated from the sub-volume 3D lung data. The descriptor distance will be calculated for the evaluation. Details will be described in the following subsection.

A. Dataset

3D volumetric chest CT exams from 48 COVID-19 cases were collected under written consent. All the cases are confirmed positive with RT-PCR test and recovered after hospitalization. The dataset includes 18 males and 30 females. Their age ranges from 24 to 75 years, with average at 51.3 years. The CT slice thickness is 1.3mm. The CT images are obtained with settings 120kVp. The current is adjusted according to the subject size.

For comparison, 3D volumetric chest CT exams from 48 normal screening cases were collected under written consent from another institute. The dataset includes 10 males and 38 females. Their age ranges from 37 to 88 years, with average at 68 years. The CT slice thickness is 1mm. The CT images are obtained with settings 120kVp/100mAs.

Firstly, the lungs of each of the 96 cases were segmented, and the segmented whole lungs were labeled/registered to the 30 Lung Marks along the axial direction. Figure 4 presents an example of CT images comparison of normal subjects (left) and Covid-19 infected subjects (right) at Lung Mark #3, #10 and #28 respectively. The manifestation of the Covid-19 is ground glass opacity, fibrous [4].

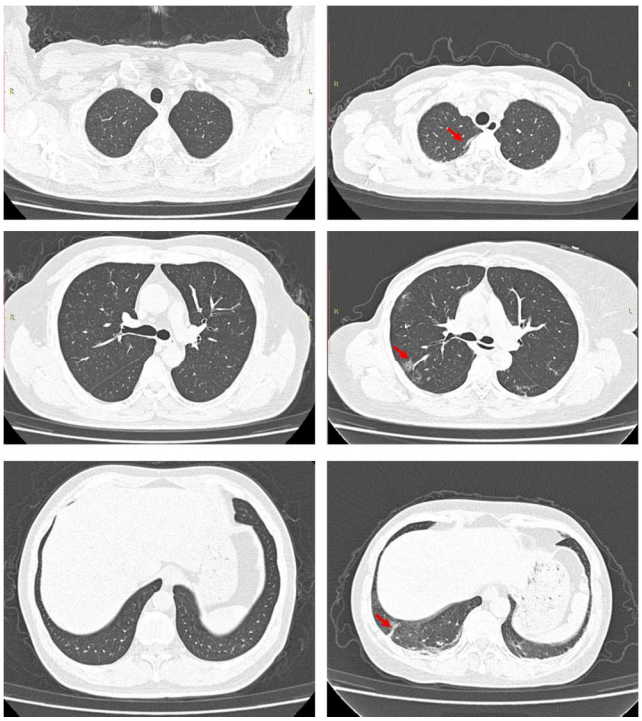

Fig. 4. CT images comparison of normal subjects (left) and Covid-19 infected subjects (right) at Lung Mark #3, #10 and #28 respectively.

B. Intensity based Texture Descriptors with Lung Mark

As described above, we computed the intensity-based texture descriptors. And then the distance between the COVID-19 and normal cases was calculated to generate the profile of distance along with Lung Mark. The average and standard deviation of the 96 cases are used to represent the distance. The results are presented in Fig. 5. Each row is a pair of comparison of traditional (left) and extended (right) Haralick features. From top to bottom are the Euclidean distance, Dice distance and Jaccard distance. The distribution is similar comparing the traditional and extended Haralick features, which shows good consistency. Comparing the three distances, we find the distribution of Euclidean distance is relatively even. The Dice and Jaccard distances have larger variation along with Lung Mark. To make a better comparison, the mean and standard deviation (std) of three distances are plotted in Fig.6. The left panel is the mean value, and the right panel is std. According to the definition of texture descriptors distance, the larger mean means the difference between COVID-19 and normal cases is larger. Smaller std means the distance according to that certain Lung Mark region more robust. Comparing to Euclidean distance, the Dice has a relative lower mean but larger std value. The Jaccard distance has a relative higher mean and higher std. Based on this observation, it is better to use the Euclidean and Jaccard distance for the classification.

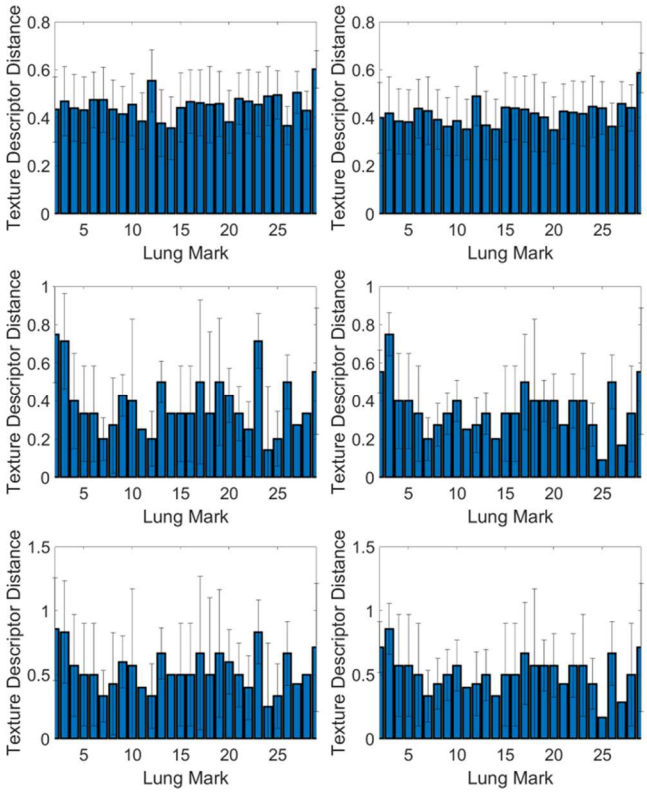

Fig. 5. Texture Descriptors Comparison with Lung Mark. Each row is a pair of comparison of traditional and extended Haralick based descriptors. From top to bottom are the Euclidean distance, Dice distance and Jaccard distance.

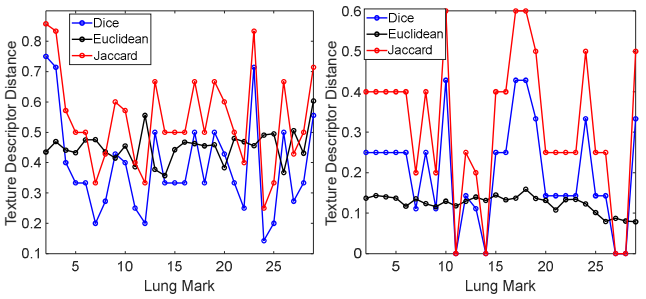

Fig. 6. Texture Descriptors Comparison with Lung Mark. Each row is a pair of comparison of traditional and extended Haralick based descriptors. From top to bottom are the Euclidean distance, Dice distance and Jaccard distance.

To demonstrate the effectiveness of the proposed method, we compare the texture descriptor distance with and without using the Lung Mark. The results are summarized in Table 1. The un-shaded part are results of traditional Haralick features. The shaded part are results of extended Haralick features. Without using Lung Mark, we extract the texture descriptors from the whole lung volume. Based on the 96 cases, we can calculate the mean and std of the descriptor distance. Using the Lung Mark, we will obtain mean and std of each Lung Mark region. To make a more comprehensive comparison, we present the maximum (Max), minimum (Min) and average (Ave) values of the Lung Marks in Table 1. It is clearly to see that the Euclidean mean without using Lung Mark is ~10 times smaller than using Lung Mark for both traditional and extended Haralick features. For the Jaccard distance, the Ave mean of Lung Mark is around 2 times larger than without Lung Mark. For the Dice distance, the Ave mean is also comparable. As we analyzed above, the larger mean value shows stronger differentiating capability. It means the using Lung Mark can give much better predication results. For comparison of std, we will mainly focus on the std of Euclidean distance since there might be zero std due to digitization for Dice and Jaccard distance. Without Lung Mark, the std is very large, around 3 times of its mean value. With Lung Mark, the std is relatively small, around 20% of its mean value. It shows the Lung Mark can reduce the feature variation prominently.

According to method section II.B, we employ n-th root mapping to normalization the magnitude in constructing the texture descriptor. In this study, three mapping roots are used including 1, 2 and 3. The comparison of texture descriptor distance using different mapping root is plotted in Fig. 7. From left to right, the mapping root increases. From top to bottom are results in Euclidean, Dice and Jaccard distance. Comparing three columns, the distribution using different mapping root is similar. However, when the root increase, the overall mean value decreases. As we discussed above, it may lower the performance. To further explore the effect of mapping root on classification, we first look at the statistical distribution of the traditional Haralick features between the normal and COCVID-19 subjects. The boxplot is presented in Fig. 8. It can be seen the 2nd and 10th dimensions are most distinguishable. Then we can compare both features across the three mapping roots. We can see when the mapping root increase, both features become less distinguishable, which agrees with our analysis above.

TABLE 1. COMPARISON OF TEXTURE DESCRIPTOR W/O LUNG MARK. THE UN-SHADED PART ARE RESULTS OF TRADITIONAL HARALICK FEATURES. THE SHADED PART ARE RESULTS OF EXTENDED HARALICK FEATURES.

Lung Mark		Without	With		
			Max	Min	Ave
Euclidean	Mean	0.0113	0.6032	0.3572	0.4528
	Std	0.0265	0.1590	0.0787	0.1237
Dice	Mean	0.5000	0.7500	0.1429	0.3874
	Std	0.0000	0.4286	0.0000	0.2007
Jaccard	Mean	0.3333	0.8571	0.2500	0.5412
	Std	0.0000	0.6000	0.0000	0.3161
Euclidean	Mean	0.0082	0.5877	0.3487	0.4165
	Std	0.0277	0.1602	0.0829	0.1281
Dice	Mean	0.3750	0.7500	0.0909	0.3593
	Std	0.0000	0.4286	0.0000	0.1548
Jaccard	Mean	0.2308	0.8571	0.1667	0.5151
	Std	0.0000	0.6000	0.0000	0.2536

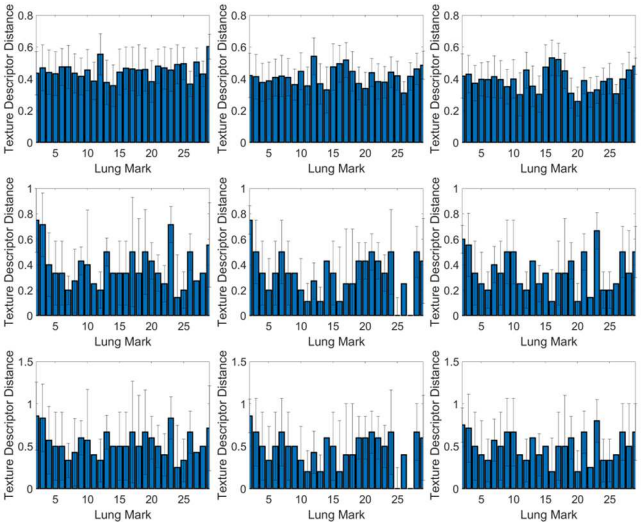

Fig. 7. Texture Descriptors Comparison with Lung Mark. Each row is a pair of comparison of traditional and extended Haralick based descriptors. From top to bottom are the Euclidean distance, Dice distance and Jaccard distance.

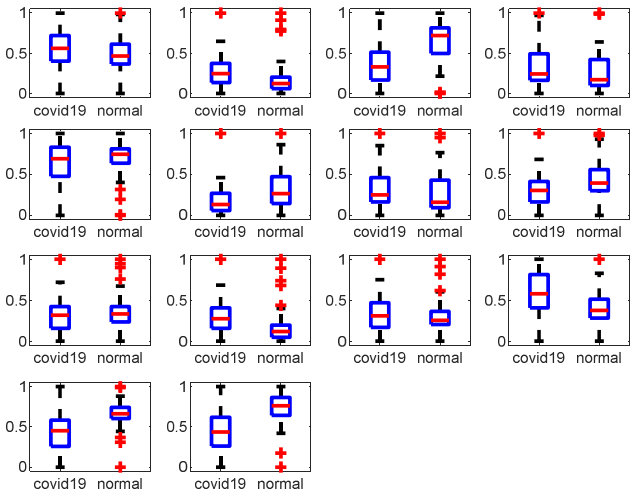

Fig. 8. boxplot of the traditional Haralick feature distribution between the normal and COCVID-19 subjects.

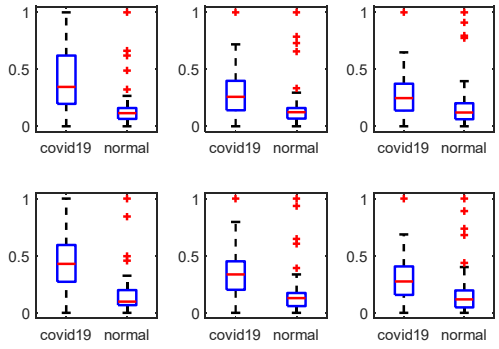

Fig. 9. boxplot of the 2nd (upper) and 10th (lower) traditional Haralick feature distribution between the normal and COCVID-19 subjects across the three mapping roots.

C. *Gradient based Texture Descriptors with Lung Mark*

We also evaluated the proposed method using the gradient based texture descriptors. Similar with the intensity-based texture descriptors, Fig. 10 shows the comparison of traditional (left) and extended (right) Haralick features. From top to bottom are the Euclidean distance, Dice distance and Jaccard distance. The texture descriptor is magnitude. Similar to the intensity-based descriptors, the profiles between the traditional and extended Haralick features are very consistent. In the following the subsection, we will only present the results based on the traditional Haralick features to make paper more concise. Comparing Fig. 10 with Fig. 5, the profile of Euclidean has larger variation comparing to the Euclidean distance of intensity-based descriptors, which indicates the gradient based descriptors are more sensitive to the Lung Mark. Comparing the Dice with Jaccard distance in Fig. 10, both bar plots have similar tendency although Jaccard distance has larger mean value. Again, the profiles along Lung Mark clearly demonstrate the feature variation along with the z-direction.

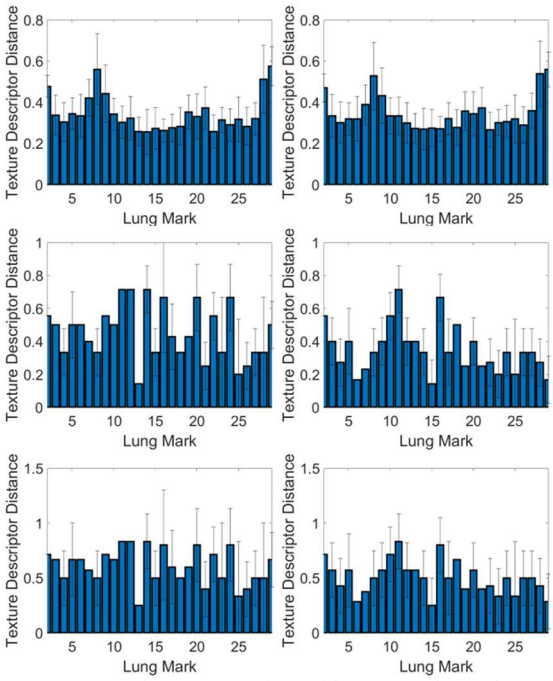

Fig. 10. Texture Descriptors Comparison with Lung Mark. Each row is a pair of comparison of traditional and extended Haralick based descriptors. From top to bottom are the Euclidean distance, Dice distance and Jaccard distance.

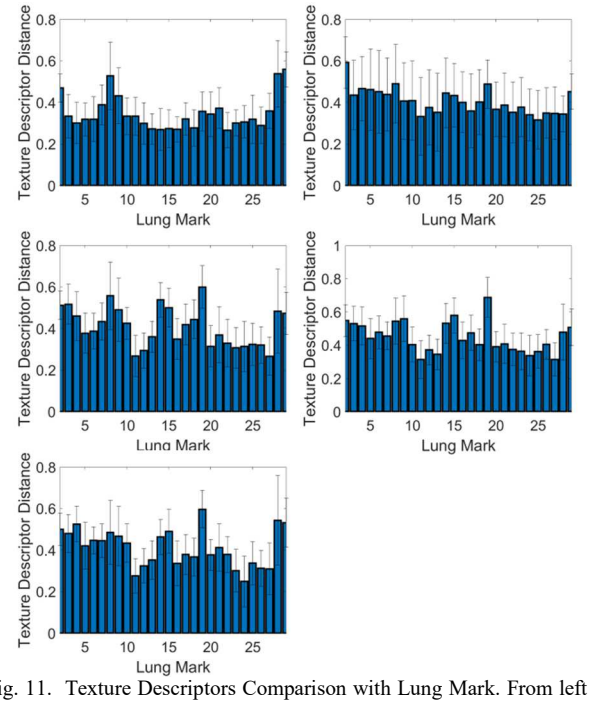

Fig. 11. Texture Descriptors Comparison with Lung Mark. From left to right, up to bottom, the results are magnitude, azimuth, polar, (azimuth, polar), (azimuth, polar, magnitude).

Since the gradient is a vector, we can obtain the vector concept texture descriptors as described in the method section. Figure 11 shows the Euclidean distance of different descriptors along with Lung Mark. From left to right, up to bottom, the results are magnitude, azimuth, polar, (azimuth, polar), (azimuth, polar, magnitude). We can see that different descriptor has different distribution. For example, a U shape distribution is observed in the magnitude descriptor from Lung Mark 7 to 30. A slope-like distribution is observed in the azimuth descriptor. The combination of azimuth and polar increase the mean value evidently comparing to each descriptor only.

TABLE 2: COMPARISON OF TEXTURE DESCRIPTOR W/O LUNG MARK OF TRADITIONAL HARALICK USING EUCLIDEAN DISTANCE.

Lung Mark		Without	With		
			Max	**Min**	**Average**
Magnitude	Mean	0.1047	0.5603	0.2667	0.3487
	Std	0.0229	0.1632	0.0611	0.0956
Azimuth	Mean	0.0870	0.5926	0.3159	0.4067
	Std	0.1109	0.1984	0.0844	0.1539
Polar	Mean	0.0846	0.6008	0.2670	0.4089
	Std	0.0288	0.2020	0.0684	0.1046
(Azimuth, Polar)	Mean	0.0159	0. 6883	0. 3133	0.4485
	Std	0.0632	0. 1680	0. 0848	0.1092
(Azimuth, Polar, Magnitude)	Mean	0.0251	0.5973	0. 2490	0.4124
	Std	0.0314	0.2150	0 0661	0.1031

To demonstrate the effectiveness of the proposed method, we also compare the texture descriptor distance with and without using the Lung Mark. The results of traditional Haralick using Euclidean distance are summarized in Table 2. Similar with Table 1, we calculate the mean and std of the descriptor

distance based on the 96 cases. Using the Lung Mark, we will obtain mean and std of each Lung Mark region. The Max, Min and Ave values of the Lung Marks are presented for comparison. For all the models, the Euclidean mean without using Lung Mark is ~10 times smaller than using Lung Mark. It means the using Lung Mark can give much better predication results. Comparing with Table 1, the std without Lung Mark becomes smaller in most model. For example, the std is 20% of its mean in magnitude model, which is also comparable with the std of using Lung Mark. However, there are also some models in which the std without Lung Mark is much larger than with Lung Mark, such as azimuth, (polar, azimuth) and so on. On the other hand, the std with Lung Mark is relative robust, which is around 40% of its mean value. To make paper more concise, the results of using Dice and Jaccard distance are presented in the APPENDIX.

IV. Conclusions

In this work, we presented an anatomic similarity inspired sensitive merit to differentiate COVID-19 cases from normal lung screen cases. The Lung Mark is proposed to convert the 3D data into 2D-like domain so that the feature variation for classification can be reduced. In the experiments, consistent results are observed across texture descriptor types and distance types in the texture measure between the normal and COVID-19 subjects. Uneven Profiles demonstrate the variation along the z-axis. With Lung Mark, the variations of texture descriptors have been reduced prominently. The Gradient based descriptor is observed more sensitive. The experimental results demonstrated the feasibility of the sensitive merit for the differentiating task.

APPENDIX

Table 3: Comparison of texture descriptor w/o Lung Mark of traditional Haralick using Jaccard distance.

Lung Mark		Without	With		
			Max	**Min**	**Average**
Magnitude	Mean	0.4286	0.8333	0.2500	0.5038
	Std	0.5000	0.5000	0.0000	0.2024
Azimuth	Mean	0.5000	0.7143	0.3333	0.5356
	Std	0.6667	0.5000	0.0000	0.3571
Polar	Mean	0.1667	0.7778	0.0000	0.3855
	Std	0.3333	0.6000	0.0000	0.2155
(Azimuth, Polar)	Mean	0.5000	0.6250	0.0000	0.4176
	Std	0.6667	0.6000	0.0.00	0.2786
(Azimuth, Polar, Magnitude)	Mean	0.6667	0.6000	0.0000	0.2817
	Std	0.0000	0.6000	0.0000	0.2017

Table 4: Comparison of texture descriptor w/o Lung Mark of traditional Haralick using Dice distance.

Lung Mark		Without	With		
			Max	**Min**	**Average**
Magnitude	Mean	0.2727	0.7143	0.1429	0.3506
	Std	0.3333	0.3333	0.0000	0.1180
Azimuth	Mean	0.3333	0.5556	0.2000	0.3706
	Std	0.5000	0.3333	0.0000	0.2279
Polar	Mean	0.0909	0.6364	0.0000	0.2630
	Std	0.2000	0.4286	0.0000	0.1330
(Azimuth, Polar)	Mean	0.3333	0.4545	0.0000	0.2671
	Std	0.5000	0.4286	0.0000	0.1738
(Azimuth, Polar, Magnitude)	Mean	0.5000	0.4286	0.0000	0.1735
	Std	0.0000	0.4286	0.0000	0.1307

References

[1] T. Ai, Z. Yang, H. Hou, C. Zhan, C. Chen, W. Lv, Q. Tao, Z. Sun and L. Xia, "Correlation of chest CT and RT-PCR testing in coronavirus disease 2019 (COVID-19) in China: A report of 1014 cases", *Radiology*, 200642, 2020.

[2] Y. Fang, H. Zhang, J. Xie, M. Lin, L. Ying, P. Pang and W. Ji, "Sensitivity of chest CT for COVID-19: Comparison to RT-PCR", *Radiology*, 200432, 2020.

[3] L. Yan and L. Xia, "Coronavirus disease 2019 (COVID-19): role of chest CT in diagnosis and management", American Journal of Roentgenology, p. 1-7, 2020.

[4] Zheng Ye, Yun Zhang, Yi Wang, Zixiang Huang and Bin Song, "Chest CT manifestations of new coronavirus disease 2019 (COVID-19): a pictorial review," *European Radiology*, pp. 1-9, 2020.

[5] D. Wang, B. Hu, C. Hu, F. Zhu, X. Liu, J. Zhang, B. Wang, H. Xiang, Z. Cheng, Y. Xiong and Y. Zhao, "Clinical characteristics of 138 hospitalized patients with 2019 novel coronavirus–infected pneumonia in Wuhan, China", JAMA, vol. 323, no, 11, pp. 1061-1069, 2020.

[6] M. Chung, A. Bernheim, X. Mei, N. Zhang, M. Huang, X. Zeng, J. Cui, W. Xu, Y. Yang, Z. Fayad and A. Jacobi, "CT imaging features of 2019 novel coronavirus (2019-bCov)", Radiology, vol. 295, no.1, pp. 202-207, 2020.

[7] J. Tan, Y. Gao, Z. Liang, W. Cao, M. Pomeroy, Y. Huo, L. Li, M. Barish, A. Abbasi and P. Pickhardt, "3D-GLCM CNN: A 3-dimensional gray-level co-occurrence matrix based CNN model for polyp classification via CT colonography", *IEEE Transactions on Medical Imaging*, early access, DIO: doi: 10.1109/TMI.2019.2963177, 2019.

[8] H. Zhang, H. Han, Z. Liang, Y. Hu, W. Moore, J. Ma, and H. Lu, "Extracting Information from Previous Full-Dose CT Scan for Knowledge-Based Bayesian Reconstruction of Current Low-Dose CT Images," *IEEE Transactions on Medical Imaging*, vol. 35, no. 3, pp. 860 - 870, 2016.

[9] Y. Gao, Z. Liang, W. Moore, H. Zhang, M. Pomeroy, J. Ferretti, T. Bilfinger, J. Ma and H. Lu, "A Feasibility Study of Extracting Tissue Textures from a Previous Full-Dose CT Database as Prior Knowledge for Bayesian Reconstruction of Current Low-dose CT Images", *IEEE Transactions on Medical Imaging*, vol. 38, no.8, pp. 1981-1992, 2019.

[10] H. Zhang, H. Han, J. Wang, J. Ma, Y. Liu, W. Moore, and Z. Liang, "Deriving Adaptive MRF Coefficients from Previous Normal-dose CT Scan for Low-dose Image Reconstruction via Penalized Weighted Least-squares Minimization," *Medical Physics*, vol. 41, no. 4, 041916-1 /041916-15 (PMCID: PMC3971828), 2014.

[11] T. Ojala, M. Pietikainen, and T. Maenpaa, "Multiresolution gray-scale and rotation invariant texture classification with local binary patterns", *IEEE Transactions on pattern analysis and machine intelligence*, vol.24, no.7, pp.971-987, 2002.

[12] J. Chen, S. Shan, C. He, G. Zhao, M. Pietikainen, X. Chen, W. Gao. WLD: A robust local image descriptor. IEEE transactions on pattern analysis and machine intelligence, vol. 32, no. 9, pp.1705-1720, 2009.

[13] D. Zhang, A. Wong, M. Indrawan and G. Lu, "Content-based image retrieval using Gabor texture features", IEEE Transactions Pami, pp. 392–395, 2000.

[14] D. Chen, R. Chang, W. Kuo, M. Chen, and Y. Huang. Diagnosis of breast tumors with sonographic texture analysis using wavelet transform and neural networks. *Ultrasound in Medicine&Biology*, vol. 28, no. 10, pp. 1301-1310, 2002.

[15] R. Haralick, K. Shanmugam, and I. Dinstein, "Textural features for image classification*," IEEE TSMC*. vol. 3, no. 6, pp. 610-621, 1973.

[16] Y. Hu, Z. Liang, b. Song, et al., "Texture feature extraction and analysis for polyp differentiation via computed tomography colonography," *IEEE TMI*. vol. 35, no. 6, pp.1522-1531, 2016.

[17] X. Tang. Texture information in run-length matrices. *IEEE Transactions on Imaging Processing*, vol. 7, pp. 11, pp. 1602-1609, 1998.

[18] G. Thibault, J. Angulo, and F. Meyer. Advanced Statistical Matrices for Texture Characterization: Application to Cell Classification. *IEEE Transactions on Biomedical Engineering*, vol. 61, no.3, pp. 630-637, 2014.

[19] C. Sun and W. G. Wee. Neighboring gray level dependence matrix for texture classification. *Computer Vision, Graphics, and Image Processing*, vol. 23, no.3, pp. 341-352, 1983.

[20] W. Cao, M. Pomeroy,vP. Pickhardt, et al., "A local geometrical metric-based model for polyp classification", *Proceedings of SPIE*: Computer-Aided Diagnosis; 1095014, 2019.

[21] P. Jaccard, "The distribution of the flora in the alpine zone", New Phytologist, vol. 11, no.2, pp. 37-50, 1921.

[22] L. Dice, "Measures of the amount of ecologic association between species", Ecology, vol.26, no.3, pp.297-302, 1945.